Boundary-Layer Meteorol (2013) 146:149–160
DOI 10.1007/s10546-012-9763-0

RESEARCH NOTE

# Statistics of the Wind-Speed Difference Between Points with Cross-Wind Separation

**J. D. Wilson**

Received: 8 February 2012 / Accepted: 2 August 2012 / Published online: 25 August 2012


**Abstract** This note reports statistics of instantaneous wind-speed differences between pairs of points in the surface layer sharing equal height ($z = 2 - 3$ m), but separated by large distances (ranging up to 70 m) along an axis transverse to the direction of the mean wind. To provide context for the analysis, some elementary statistical properties of point-point signal differences are first derived, then, on the basis of observations from a transect of anemometers, correlations are provided that allow an estimate of the root-mean-square daytime speed difference. During unstable daytime conditions the prevalence of eddies of a scale larger than instrument separation ensured paired instruments sampled highly correlated winds, whereas at night paired instruments sampled weaker fluctuations (largely) independently. The probability density function of the wind-speed difference proved roughly invariant with respect to the micrometeorological state, and tends towards a Gaussian as separation becomes large.

**Keywords** Atmospheric surface-layer winds · Statistics of differences · Structure function · Wind-speed differences

## 1 Introduction

It may be useful in some contexts to anticipate the likely magnitude of instantaneous near-ground wind-speed differences, between points in the horizontal plane with separation transverse to the wind: for instance anemometers are sometimes inter-calibrated by mounting them at equal heights in a line across the wind, and wind turbines experience fatigue due to "rotational sampling" of the spatially non-uniform wind. The operation at Dugway Proving Grounds, Utah (23 May – 2 June 2005) of a transect of sonic anemometers at fixed height provided the opportunity to extract the statistics of wind-speed difference during many intervals when the anemometer separation was approximately perpendicular to the mean wind (see Fig. 1). Many previous authors have analyzed signals from an array of anemometers standing

J. D. Wilson (✉)
Department of Earth and Atmospheric Sciences, University of Alberta, Edmonton, AB T6G 2E3, Canada
e-mail: jaydee.uu@ualberta.ca

**Fig. 1** View of the site for the Dugway2005 experiment, looking towards the north-west. The sonic anemometers of the transect are in the configuration with $\eta = 3$ m separations, at a height of 2.14 m, and all west of the main tower (whereas for the majority of the data analyzed here, the transect configuration was $\eta = 10$ m, $z = 3$ m). Winds blew very reliably from the north over a uniform desert surface extending many tens of km upwind

in a line across the wind, but most (e.g. Ropelewski et al. 1973; Kristensen et al. 1981; Mann 1994; Tong and Wyngaard 1996) have focused on the spectral coherence of the horizontal velocity fluctuations (loosely, correlation coefficient as a function of eddy frequency), while others (e.g. Flay and Stevenson 1988) have reported turbulence length scales or (e.g. Castaing et al. 1990) the probability density function (PDF) of velocity differences at small separation in relation to the fine-scale structure of turbulence.

After briefly covering pertinent statistical and meteorological theory, this note gives observed spectra and PDFs of wind-speed difference as a function of crosswind separation, and develops a qualitative basis for estimating the variance of the wind-speed difference.

## 2 Theory

### 2.1 Statistics of Signal Differences

Some useful guidance on the statistical properties of point–point signal differences can be derived from elementary considerations. Consider signals $q_1(t)$, $q_2(t)$ at two points sharing the same height $z$, but separated by a crosswind ($y$) distance of magnitude $\Delta y = \eta$, in a horizontally-homogeneous boundary layer. The PDF $f(\Delta)$ for the difference $\Delta = q_1 - q_2$ must be symmetric about $\Delta = 0$. The positive 'side' of $f(\Delta)$ must equal one half the PDF of $|q_1 - q_2|$, all odd moments of $f(\Delta)$ vanish, and accordingly the lowest non-trivial moments of the difference signal are the variance $\sigma_\Delta^2$ (loosely equivalent to a second-order structure function for transverse separation, e.g. Wyngaard 2010, p. 152) and the kurtosis $K_\Delta$.

The moment generating function (MGF) of the signal difference is by definition (Hogg and Craig 1978)

$$M_\Delta(p) \equiv \int_{-\infty}^{\infty} e^{p\Delta} f(\Delta) d\Delta = 1 + p\overline{\Delta} + \frac{1}{2!}p^2\overline{\Delta^2} + \cdots \tag{1}$$

where $p$ is an abstract transform variable, the overbar denotes an average value, and $\overline{\Delta^2} \equiv \sigma_\Delta^2$ is the variance of the signal difference; strictly these are moments about zero, but in the present case the mean ($\overline{\Delta}$) vanishes, as symmetry implies $\overline{\Delta^{2n+1}} = 0$ for all $n \geq 0$. For sufficiently far-separated points it is reasonable to assume $q_1(t)$, $q_2(t)$ are independent, in which limit[1] it is easy to show that

$$M_\Delta(p) = M_{q_1}(p) M_{q_2}(-p) \tag{2}$$

(Hogg and Craig 1978; Freund 1992). From Eq. 2 one may deduce by straightforward algebraic manipulation[2] that if the observation points are sufficiently far separated to justify the assumption of independence of $q_1$, $q_2$ (and bearing in mind that, under the assumed condition of horizontal homogeneity, single-point velocity statistics at locations 1 and 2 are identical), the two lowest order non-zero moments of (any) signal difference (on a horizontal plane) are

$$\sigma_\Delta^2 = 2\sigma_q^2, \tag{3}$$

$$K_\Delta = \frac{3}{2} + \frac{1}{2}K_q, \tag{4}$$

where $\sigma_q$ is the standard deviation of the signal at $z$, and $K_q$ its kurtosis

$$K_q = \overline{(q - \overline{q})^4}/\sigma_q^4. \tag{5}$$

Equation 3 gives an upper limit to the variance of the difference signal. On the other hand $\sigma_\Delta^2$ obviously must vanish in the limit $\eta \to 0$ (vanishing separation). Therefore observed values of

$$\phi^2(\eta) \equiv \frac{\sigma_\Delta^2(\eta)}{2\sigma_q^2} = \frac{\overline{(q'(y) - q'(y+\eta))^2}}{2\sigma_q^2} \tag{6}$$

must lie in the range $0 \leq \phi^2 \leq 1$, where $\phi^2$ is a unique function

$$\phi^2 \equiv 1 - C(\eta) \tag{7}$$

of the correlation coefficient

$$C(\eta) = \frac{\overline{q'(y)q'(y+\eta)}}{\sigma_q^2} \tag{8}$$

[1] Generally if $\omega = ax + by$ where $a, b$ are constants and $x, y$ are random variables that are independent but not necessarily identically distributed, the MGF for $\omega$ is $M_x(ap)M_y(bp)$, where $M_x, M_y$ are the MGFs for $x, y$. In the words of Hogg and Craig (1978), "stochastic independence of $X_1$ and $X_2$ implies that the moment-generating function of the joint distribution factors into the product of the moment-generating functions of the two marginal distributions."

[2] Evaluate each of the MGFs on the right-hand side of Eq. 2 by substituting the series in $p$ (or $-p$), cross multiply, and express the result as an ordered sequence $a_n p^n$ of powers of $p$ (coefficients $a_n$ of odd powers will vanish); then equate each coefficient to its equivalent on the right-hand side of Eq. 1.

between signal fluctuations at points $y$, $y+\eta$. The quantity $\phi^2$ is essentially a (normalized) second-order structure function (the abstract signal fluctuation $q'$ here substitutes for the more usual *velocity* fluctuation component $u'$ or $v'$). For any given averaging interval, $\phi(\eta)$ should increase monotonically with increasing separation $\eta$; while for fixed $\eta$, over a large number of runs in varying meteorological conditions $\phi$ should decrease with increasing ratio $\Lambda_y/\eta$ of the transverse integral length scale to the separation.

These considerations apply to any spatial difference signal (and, for that matter, to differences in *time* rather than space, if the turbulence is stationary), however the analysis of Sect. 4 addresses wind-speed differences,[3] and in the balance of this note $\Delta$ is to be understood as being a wind-speed difference, and $\phi$ as its normalized standard deviation. One might expect that at high mean wind speeds the PDF of wind speed may (to a first approximation) be Gaussian, in which case the kurtosis of wind speed $K_s = 3$. Then in turn—according to Eq. 4, which applies only provided the sampling points are sufficiently far separated—the kurtosis of wind-speed difference $K_\Delta = 3$, and the PDF of wind-speed difference also should be close to Gaussian, thus, adequately characterized by $\sigma_\Delta$.

### 2.2 Existing Semi-empirical Theory for Velocity Differences

The classic Kolmogorov (1941)–Obukhov (1941) paradigm $\phi^2 \propto \eta^{2/3}$ for velocity structure functions, applicable (at best) for small anemometer separations, hardly needs introduction and will be compared below with the present data. Existing semi-empirical formulations of velocity spectra and cospectra, to the extent that they are realistic, should encapsulate the statistics of wind-speed and velocity differences. Mann (1994) invoked rapid distortion theory to develop an approximate relation for the spectral tensor $\Phi_{ij}(\mathbf{k})$ of neutral atmospheric surface-layer turbulence ($\mathbf{k}$ being the wavenumber vector; the mean shear was approximated as being height-invariant), and compared computations based on his model spectra with the lateral coherency of the longitudinal wind component measured by sonic anemometers with crosswind separations $\eta = 15$, 32 and 47.5 m at height $z = 70$ m (agreement was reasonably good, presumably at least in part because the model involved several optimizable coefficients). Tong and Wyngaard (1996) adapted the two-dimensional spectral model of Peltier et al. (1996) for stratified surface-layer flow, and computed a lateral coherency spectrum that agreed well with measurements from sonic anemometers with crosswind separation $\eta \approx 0.5$ m at height $z = 10$ m.

## 3 Measurements and Analysis

Eighteen Campbell Scientific CSAT3 sonic anemometers (path length $\approx 0.12$ m; output at 20 Hz) were operated over a dry lakebed (Fig. 1). Nine were mounted on a 29 m tower (at heights $z = 1.42$, 2.14, 3.00, 4.26, 6.14, 8.81, 12.52, 17.94, 25.69 m), and the balance on a (nominally east-west) crosswind transect, either at height $z = 3.00$ m with separations $\eta = 10$ m, or at $z = 2.14$ m with $\eta = 3$ m. Previous authors (e.g. McNaughton et al. 2007; Metzger and Holmes 2008; Wilson 2008; Charuchittipan and Wilson 2009) provide information on the site (nominal coordinates 113°27.07′W; 40°8.1′N; 1296 m above sea level) and on the measurement system. The dry lake bed (roughness length 0.2–0.5 mm) extended for

[3] The choice to examine differences in wind speed rather than longitudinal velocity $u'$ was made in the light of uncertainty as to the degree of consistency in orientation of the sonic anemometers on the transect. These were moved during the experiment, some more than once, and hurriedly.

many tens of km upwind from (i.e. north of) the installation. All anemometers were oriented to face (nominal) north, and wind direction $\beta$ is here defined such that $\beta = 0°$ corresponds to a northerly wind (i.e. perpendicular to the transect).

As noted by Wilson (2008) however, the tower and transect had been installed near a raised parking area on which stood several large instrument trailers (see McNaughton et al. 2007, for a photograph of the set-up), and the influence of these obstacles could readily be detected. To exclude instruments in the disturbed flow, here the analysis is restricted to those sonics standing at least 20 m west of the tower or mounted at one of the four uppermost tower levels.

For each run (duration 30 min) the friction velocity, turbulent temperature scale and Obukhov length, which together characterize the state of the surface layer, were computed according to

$$u_*^4 = \left(\overline{\overline{u'w'}}\right)^2 + \left(\overline{\overline{v'w'}}\right)^2, \tag{9}$$

$$T_* = -\overline{\overline{w'T'}}/u_*, \tag{10}$$

$$L = \frac{u_*^2 T_0}{k_v g T_*}, \tag{11}$$

where $\overline{\overline{w'T'}}$ denotes the average value of the kinematic heat flux density $\overline{w'T'}$ over the four uppermost sonics on the tower (etc), $k_v$ is the von Karman constant (taken as 0.4), $g$ is the acceleration due to gravity and $T_0$ is the mean temperature (K). Prior to the extraction of these statistics a double coordinate rotation, sequentially enforcing $\overline{v} = 0$ then $\overline{w} = 0$ (e.g. Wilczak et al. 2001) had been performed individually for each anemometer. In the analysis to follow the selection criteria, unless otherwise mentioned, were: $u_* \geq 0.15\,\mathrm{m\,s^{-1}}$, mean wind direction $|\beta| \leq 15°$ (assuring the east-west anemometer transect ran "perpendicular" to mean wind direction) and $L \leq 0$. Please note that, unlike some earlier authors who focus on the "cup" wind speed $s = \left(u^2 + v^2\right)^{1/2}$ (e.g. Bernstein 1967; Van Den Hurk and De Bruin 1995), we here define wind speed as $s = \left(u^2 + v^2 + w^2\right)^{1/2}$, where $(u, v, w)$ are the velocity components in the meteorological convention.

## 4 Observed Statistics of Wind-Speed Difference

### 4.1 PDF and Spectrum of Wind-Speed Difference

The PDF of wind-speed difference $\Delta$ was computed for each selected run, as follows. At each instant in time, one or more pairs of sonics (labels: $j, k$) having given separation $\eta$ provided samples of the wind-speed difference $\Delta \equiv s'_j - s'_k$, where differencing of the fluctuations (rather than the full instantaneous values) corrects for any residual offset in calibration (and also, to some degree, corrects for any unsuspected lateral inhomogeneity of the flow). For each separation $\eta$, the available samples were standardized as $|\Delta|/\sigma_\Delta$, and the PDF of this variate, computed in 99 bins spanning $0 \leq |\Delta|/\sigma_\Delta \leq 5$, was assumed to represent (twice) the positive side of the PDF of $\Delta/\sigma_\Delta$.

Figure 2 shows that the PDF of the normalized wind-speed difference $(\Delta/\sigma_\Delta)$ is non-Gaussian, but that (as speculated in Sect. 2) it converges towards a Gaussian with increasing separation. The excessive peak (relative to a Gaussian) at $\Delta s/\sigma_{\Delta s} = 0$ identifies the distribution of wind-speed difference as being leptokurtic, i.e. its kurtosis >3, the value for the

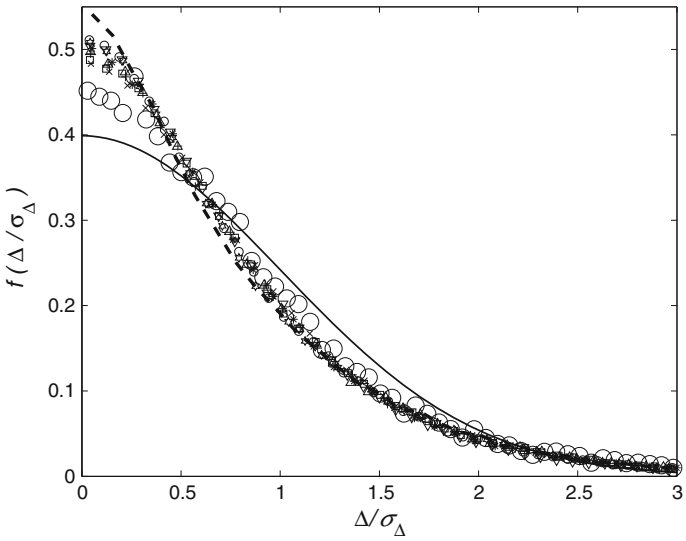


**Fig. 2** Positive side of the PDF for the normalized difference in wind speed $\Delta/\sigma_\Delta$. The *solid line* is a standardized Gaussian. *Dashed line*, $\eta = 3$ m. *Small symbols*, $\eta = 10$ m (showing the eight runs of the afternoon of 24 May). *Large circle symbol* $\eta = 40$ m (corresponds to run denoted *circle* for 10-m separation). Each 30-min PDF plotted was based on $N = 108{,}000$ samples ($\eta = 3$ m), $N = 144{,}000$ samples ($\eta = 10$ m), or $N = 36{,}000$ samples ($\eta = 40$ m)

Gaussian: understandably for small separations there is a high probability of the wind-speed difference being very small.

Figure 3 displays power spectra of the wind-speed difference for separations $\eta = (10, 20, 30, 40)$ m, from a 60-min interval for which $u_* = 0.21\,\mathrm{m\,s^{-1}}$, $L = -3.5$ m, mean wind speed at instrument height $\overline{s} = 4.77\,\mathrm{m\,s^{-1}}$, and ABL depth $\delta \approx 1$ km. Spectra were computed by fast Fourier transform based on $2^{16}$ points (sampled at 20 Hz, covering $T = 54.61$ min); in each case the $2^{16}$ points were divided into 16 sub-blocks of $2^{12}$ points, and each spectral estimate plotted is the average of the sixteen sub-block spectra. At high frequency the spectra are contaminated by aliasing. All four spectra coincide above about 0.1 Hz, with slope $\mathrm{d}\ln(fS)/\mathrm{d}\ln f \approx -2/3$ where $0.1 \lesssim f \leq 0.5$ Hz, implying that, in this region, $S_\Delta(f) \propto f^{-5/3}$. In the energy-containing region the spectral density decreases with decreasing separation of the instruments (but for the contribution of noise, the variance must vanish in the limit $\eta \to 0$). As instrument separation increases the spectral peak for wind-speed difference shifts toward lower frequency, although the peaks roughly coincide if plotted on a normalized frequency axis $n = f\eta/\overline{u}$ (not shown).

### 4.2 Second Moment of the PDF of Wind-Speed Difference

As expected, root-mean-square speed differences $\sigma_\Delta$ proved broadly proportional to the mean wind speed $\overline{s}$, and for the present measurements generally $\sigma_\Delta/\overline{s} \sim 0.1$–$0.2$. Figure 4 summarizes the values of $\sigma_\Delta/u_*$ under unstable stratification, for all available separations. Although few runs with separations $\eta < 10$ m met the selection criteria, those results do hint at the expected reduction in $\sigma_\Delta/u_*$ with decreasing separation. For separations $\eta \geq 10$ m, the limiting neutral value is about 3.0—more specifically the best-fit neutral values of $\sigma_\Delta/u_*$ for

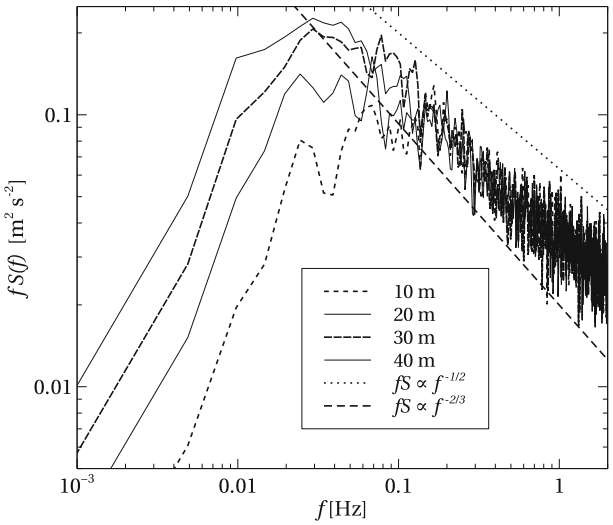


**Fig. 3** Spectra of the wind-speed difference between sonic anemometers at equal height ($z = 3$ m) but separated in the cross-wind direction by distances $\eta = 10, 20, 30, 40$ m. Observed at Dugway Proving Grounds during the hour starting 1430 MDT 24 May 2005. Surface-layer conditions: $u_* = 0.21\ \mathrm{m\,s^{-1}}$, $L = -3.5$ m, mean wind speed at instrument height $\overline{s} = 4.77\ \mathrm{m\,s^{-1}}$

$\eta = 10, 20, \ldots 70$ m were respectively (2.7, 3.0, 3.1, 3.2, 2.8, 2.7, 2.7), with greater uncertainty in the latter three values. Thus, tentatively, the trend to increasing $\sigma_\Delta$ with increasing separation can be detected, but for $\eta >> 1$ m it is rather a weak trend.

Figure 5 gives the diurnal cycle of $\phi = \sigma_\Delta/(\sqrt{2}\sigma_s)$ for fixed $\eta/z = 10/3$, over three consecutive days of the experiment. As they must, values of $\phi$ lie in the range $0 \le \phi \le 1$, and assume minimum values during daytime (large $\delta/|L|$) that are roughly invariant from day to day, with a value of about 0.4 (note: a limited range of conditions was sampled on these three consecutive and rather similar days).

Figure 6 is a plot of observed $\phi^2$ versus $\eta/z$, along with previously proposed formulae. The Kolmogorov (1941)–Obukhov (1941) paradigm $\phi^2 \propto \eta^{2/3}$, shown by long dashed lines fitted on both panels of Fig. 6, is expected to apply (at best) for "observation points located at a distance apart that exceeds the internal scale of turbulence, but is small by comparison with the distance to the boundary of the flow" (Obukhov 1962), and (along with innumerable wind-tunnel confirmations) it was first verified for small separations in the atmospheric surface layer ($\eta \le 0.6$ m at heights $z = 1.5, 3, 15$ m) by Obukhov and Yaglom (1959). On the evidence of Fig. 6 it does not apply for $\eta/z > 5$, however it provides a reasonable fit for narrower separations $\eta < 5$.

There have been few experimental studies of the transverse structure function (or correlation coefficient) for large separations, and particularly so in the atmosphere (Kader et al. (1989), noted that "most of the old measurements cover only a limited range of small distances either belonging to the inertial subrange or being only slightly longer than the large-scale limit of this subrange"). Mestayer (1982) reported transverse structure functions

$$B_{nn}(\eta) = \frac{\overline{(u'(y) - u'(y+\eta))^2}}{\sigma_u^2} \tag{12}$$

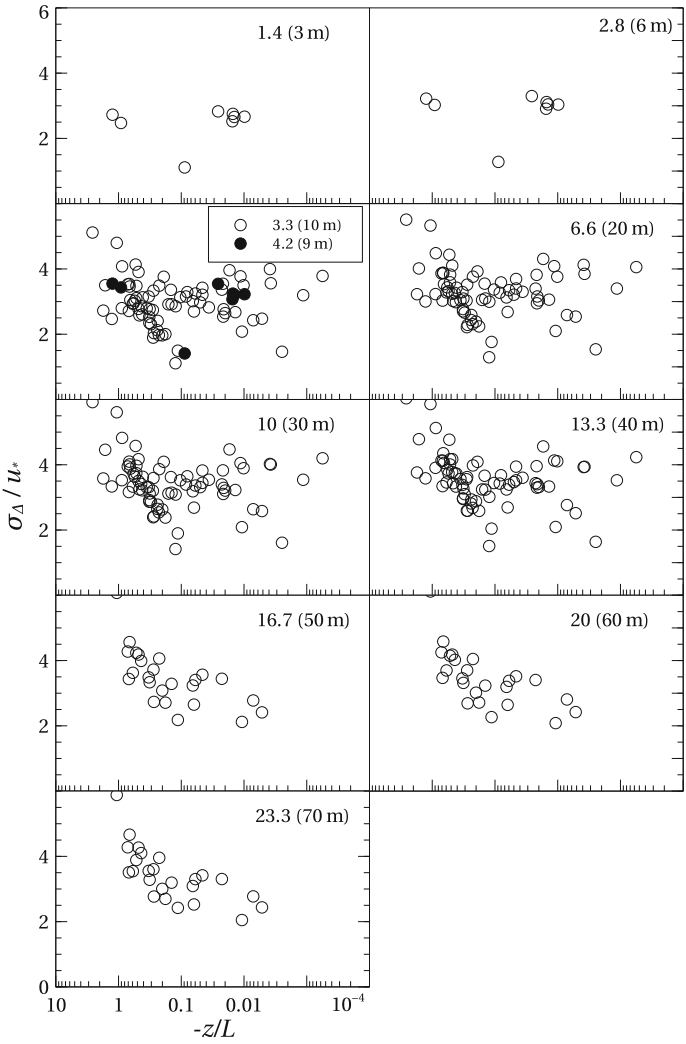


**Fig. 4** Observed values of normalized standard deviations of wind-speed differences $\sigma_\Delta/u_*$ for all available separations (30-min runs, unstable stratification). *Legend* gives separation normalized by observational height (dimensional separation in *brackets*)

of the longitudinal velocity fluctuation in a boundary-layer wind tunnel, finding $B_{nn}(\eta) \propto \eta^{2/3}$ for $50 \lesssim \eta/\eta_K \lesssim 1000$ ($\eta_K$ being the Kolmogorov microscale). Others studying the homogeneous shear layer in a wind tunnel (e.g. Garg and Warhaft 1998; Ferchichi and Tavoularis 2000) report that Kolmogorov-Obukhov scaling applies over a more limited range in $\eta/\eta_K$ (roughly 30–100). Interpretation of these findings demands attention to detail (e.g. Reynolds number, measurement height) and need not be pursued here.

Returning to atmospheric measurements and Fig. 6, Kader et al. (1989) reported the lateral correlation coefficient measured at a height of 3.2 m in the neutral surface layer during a single 120-min interval, with anemometer crosswind separations spanning 3–32 m ($1 \lesssim \eta/z \leq 10$), and fitted it with a semi-empirical curve (which they had derived in the context of

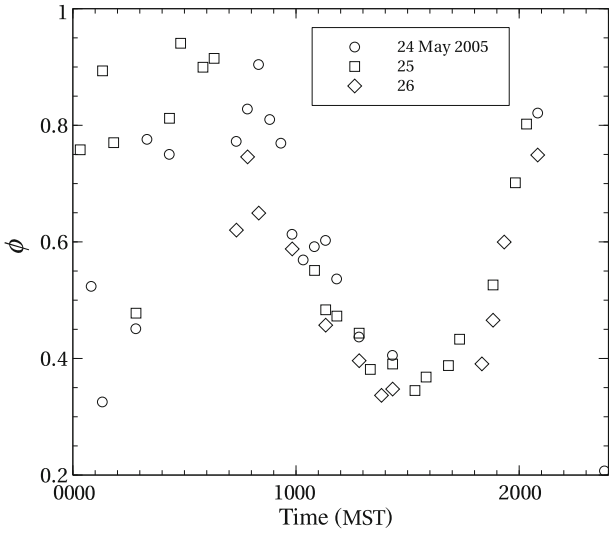


**Fig. 5** Diurnal cycle in $\phi = \sigma_\Delta/(\sqrt{2}\sigma_s)$ for separation $\eta = 10$ m ($\eta/z = 3.3$). MST is Mountain Standard Time (on May 24 sunrise occurred at 0603, sunset at 2046). Selection criteria on friction velocity and Obukhov length are relaxed

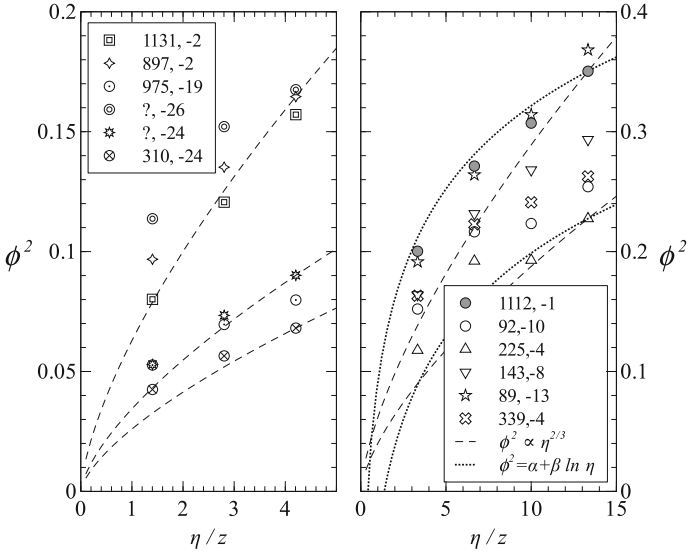


**Fig. 6** $\phi^2 \left(\equiv \sigma_\Delta^2/(2\sigma_s^2)\right)$ versus normalized crosswind separation of the two anemometers $\eta/z$. *Left panel* anemometer height $z = 2.14$ m and transverse spacing $\eta = 3$ m; Kolmogorov curves forced to run through the observations at $\eta/z = 4.21$. *Right panel* data for the afternoon of 24 May with anemometer height $z = 3$ m and transverse spacing $\eta = 10$ m; curves forced to run through the observations at $\eta/z = 13.3$ ($\beta = 0.1$ in the Kader et al. 1989 relation). *Legend* gives $-\delta/L$, $L$ (where $\delta$ was estimated by the method of Wilson (2008), and $L$ is given in m)

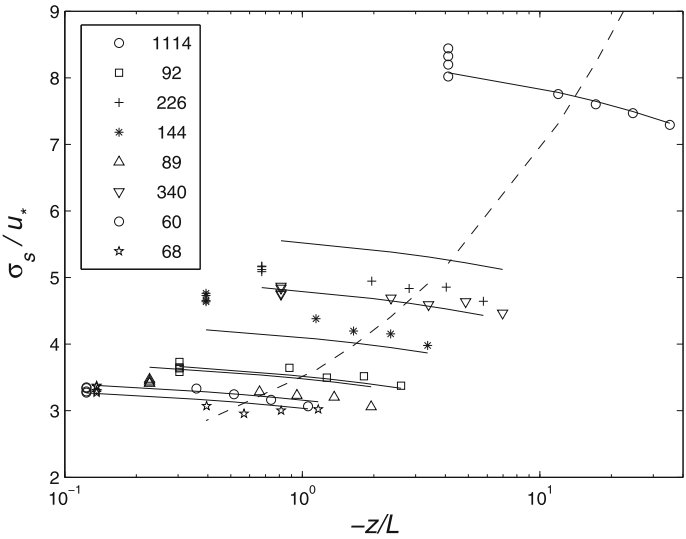


**Fig. 7** $\sigma_s/u_*$ vs. $z/L$ on the afternoon of 24 May. *Legend* gives $\delta/|L|$. The *solid lines* are Eq. 13, with ($a = 1.51, b = 0.67, c = 0.36$). The *dashed line* is Eq. 14, which does not account for the $\delta/|L|$ dependence

longitudinal correlations) whose form, in the terminology of this paper, was $C(\eta) = \alpha - \beta \ln \eta/z$. This law, which is represented by dotted lines on the right hand panel of Fig. 6, appears to be broadly consistent with the present observations. However, it cannot be correct for very large $\eta$ as it implies negative $C$, and thus values of the structure function exceeding twice the velocity variance.

### 4.3 Standard Deviation of Wind Speed

Having established (albeit only qualitatively) the behaviour of the normalized r.m.s. speed difference $\phi$ in the unstable surface layer, it remains to provide a relation for the standard deviation $\sigma_s$ of wind speed, so that an estimate of $\phi$ can be unscaled to produce the r.m.s. speed difference $\sigma_\Delta$. Figure 7 shows the values of $\sigma_s/u_*$ during the afternoon of 24 May (a period for which plausible estimates of $\delta$ are available). An empirical fit to these observations is given by

$$\frac{\sigma_s^2}{u_*^2} = \left[a + b\left(\frac{\delta}{-L}\right)^{2/3}\right]\left[1 - \left(\frac{z}{\delta}\right)^c\right], \quad L < 0, \tag{13}$$

with (rounded) best least-squares coefficients ($a = 1.51, b = 0.67, c = 0.36$). The optimization was done giving equal weight to all data points, and the coefficients were searched with resolution 0.01 (if one imposes $b = 2/3$ and $c = 1/3$, then optimal $a = 2.1$; or if, following Wilson (2008), one imposes $c = 1/4$ then optimally $a = 1.6, b = 0.8$). De Bruin et al. (1993) proposed a simpler relation

$$\frac{\sigma_s}{u_*} = 2.2\left(1 - 3\frac{z}{L}\right)^{1/3} \tag{14}$$

that lacks a $z/\delta$ dependence (see also Van Den Hurk and De Bruin 1995), and this is also plotted alongside the present data.

## 5 Conclusion

This note goes some way towards quantifying the instantaneous non-uniformity of the wind in a (statistically) uniform (i.e. horizontally homogeneous) surface layer. To anticipate wind-speed differences for separation $\eta$, begin by evaluating the standard deviation of wind speed $\sigma_s$ according to Eq. 13. Then, based on $\eta/z$ and a broad stability classification, use Figs. 5 and 6 to estimate $\phi$ and (thence) $\sigma_\Delta \equiv \sqrt{2}\phi\sigma_s$.

**Acknowledgements** The Dugway2005 experiment was a joint effort by faculty, staff and students from several institutions: University of Utah, University of Edinburgh, University of Minnesota, University of Melbourne, University of Alberta, and Imperial College London. K. McNaughton and R. Clement (School of Geosciences, U. Edinburgh) planned and supervised the sonic anemometer array; E. Swiatek and the late B. Tanner (Campbell Scientific Inc.) provided comprehensive assistance (including calibration of the anemometers); D. Storwold and J. Bowers (U.S. Army Dugway Proving Ground) provided infrastructure and support; and J. Klewicki (Mechanical Engineering, U. Utah) served as overall coordinator. JDW's participation and equipment were funded by the Natural Sciences and Engineering Research Council of Canada.

## References

Bernstein A (1967) A note on the use of cup anemometers in wind profile experiments. J Appl Meteorol 6:280–286

Castaing B, Gagne Y, Hopfinger EJ (1990) Velocity probability density functions of high Reynolds number turbulence. Phys D 46:177–200

Charuchittipan D, Wilson J (2009) Turbulent kinetic energy dissipation in the surface layer. Boundary-Layer Meteorol 132:193–204

De Bruin H, Kohsiek W, van den Hurk B (1993) A verification of some methods to determine the fluxes of momentum, sensible heat, and water vapour using standard deviation and structure parameter of scalar meteorological quantities. Boundary-Layer Meteorol 63:231–257

Ferchichi M, Tavoularis S (2000) Reynolds number effects on the fine structure of uniformly sheared turbulence. Phys Fluids 12:2942–2953

Flay R, Stevenson D (1988) Integral length scales in strong winds below 20 metres. J Wind Eng Ind Aerodyn 28:21–30

Freund J (1992) Mathematical statistics, 5th edn. Prentice-Hall, Upper Saddle River, 658 pp

Garg S, Warhaft Z (1998) On the small scale structure of simple shear flow. Phys Fluids 10:662–673

Hogg R, Craig A (1978) Introduction to mathematical statistics, 4th edn. Macmillan, New York, 438 pp

Kader B, Yaglom A, Zubkovskii S (1989) Spatial correlation functions of surface-layer atmospheric turbulence in neutral stratification. Boundary-Layer Meteorol 47:233–249

Kolmogorov A (1941) The local structure of turbulence in incompressible viscous fluid for very large Reynolds numbers. Dokl Akad Nauk SSSR 30(4). Reprinted in Proc R Soc Lond A (1991) 434:9–13; and in Turbulence and stochastic processes. Cambridge University Press, Cambridge

Kristensen L, Panofsky H, Smith S (1981) Lateral coherence of longitudinal wind components in strong winds. Boundary-Layer Meteorol 21:199–205

Mann J (1994) The spatial structure of neutral atmospheric surface-layer turbulence. J Fluid Mech 273:141–168

McNaughton K, Clement R, Moncrieff J (2007) Scaling properties of velocity and temperature spectra above the surface friction layer in a convective atmospheric boundary layer. Nonlinear Process Geophys 14:257–271

Mestayer P (1982) Local isotropy and anisotropy in a high-Reynolds-number turbulent boundary layer. J Fluid Mech 125:457–503

Metzger M, Holmes H (2008) Time scales in the unstable atmospheric surface layer. Boundary-Layer Meteorol 126:29–50

Obukhov A (1941) On the distribution of energy in the spectrum of turbulent flow. Dokl Akad Nauk SSSR 32(1):22–24

Obukhov A (1962) Some specific features of atmospheric turbulence. J Fluid Mech 13:77–81

Obukhov A, Yaglom A (1959) On the microstructure of atmospheric turbulence—a review of recent work in the U.S.S.R. Q J R Meteorol Soc 85:81–90

Peltier L, Wyngaard J, Khanna S, Brasseur J (1996) Spectra in the unstable surface layer. J Atmos Sci 53:49–61
Ropelewski C, Tennekes H, Panofsky H (1973) Horizontal coherence of wind fluctuations. Boundary-Layer Meteorol 5:353–363
Tong C, Wyngaard J (1996) Two-point coherence in the atmospheric surface layer. Boundary-Layer Meteorol 81:105–121
Van Den Hurk B, De Bruin H (1995) Fluctuations of the horizontal wind under unstable conditions. Boundary-Layer Meteorol 74:341–352
Wilczak J, Oncley S, Stage S (2001) Sonic anemometer tilt correction algorithms. Boundary-Layer Meteorol 99:127–150 (Note the typographic error in Eq. 33—a missing factor of 1/2)
Wilson J (2008) Monin–Obukhov functions for standard deviations of velocity. Boundary-Layer Meteorol 129:353–369
Wyngaard J (2010) Turbulence in the atmosphere. Cambridge University Press, Cambridge, 393 pp